

Theoretical Study of Dioxygen Binding Process in Iron(III) Catechol Dioxygenase: “Oxygen Activation” vs “Substrate Activation”

Naoki Nakatani,[†] Yoshihide Nakao,[†] Hirofumi Sato,[†] and Shigeyoshi Sakaki^{*,†,‡}

Department of Molecular Engineering, Graduate School of Engineering, Kyoto University, Kyoto-Daigaku-Katsura, Nishikyo-ku, Kyoto 615-8510, Japan, and Fukui Institute for Fundamental Chemistry, Kyoto University, Takano Nishibiraki-cho, Sakyo-ku, Kyoto 606-8103, Japan

Received: July 23, 2008; Revised Manuscript Received: February 2, 2009

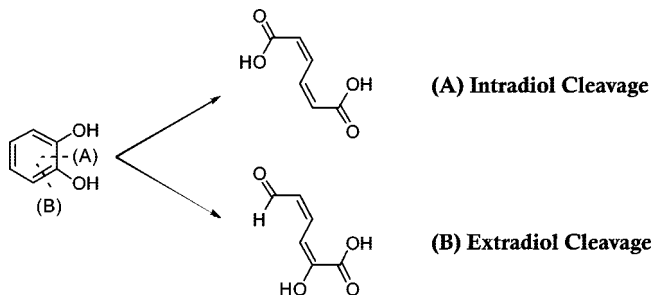
Dioxygen binding process of nonheme iron(III) center in intradiol catechol dioxygenase was investigated with CASSCF/CASPT2 method to incorporate multiconfigurational character participating in Fe–O₂ interaction. In this process, two alternative mechanisms were proposed: one is called “oxygen activation” and the other is called “substrate activation”. Our CASSCF/CASPT2-calculated results support the oxygen activation. Potential energy curves and electronic structure evaluated with SA(state-averaged)-CASSCF/CASPT2 method indicate that the charge transfer directly occurs from the catecholate moiety to the dioxygen moiety in the O₂ binding process, to produce η^1 -end-on type iron(III)–superoxo complex. This is the key step of the dioxygen activation. Interestingly, the iron center always keeps high spin d⁵ character during the O₂ binding process, indicating the iron(III) center does not receive charge transfer from the catecholate moiety. However, this does not mean that the iron(III) center is not necessary to the dioxygen activation. The important role which the iron(III) center plays in catechol dioxygenase is to adjust the energy level of O₂ to induce the charge transfer from the catecholate moiety to the dioxygen moiety. Besides the η^1 -end-on iron(III)–superoxo complex, η^2 -side-on type iron(III)–superoxo complex is also optimized. This species is more stable than the η^1 -end-on type iron(III)–superoxo complex, suggesting that this is considered as a stable isomer in the early stage of the catalytic cycle.

Introduction

Catechol dioxygenases, found in a diverse range of soil bacteria, activate dioxygen molecules and catalyze the aromatic bond cleavage of catechol (1,2-dihydroxylbenzene) and its derivatives.^{1–5} Their oxygenation catalyses are of considerable interest, as follows: the aromatic bond cleavage is in general difficult because of its considerably large stability due to the resonance structure. Also, dioxygen molecule is not reactive to most of organic compounds, because dioxygen molecule has triplet ground state but most of organic molecules have closed-shell singlet ground state. In spite of these difficulties, catechol dioxygenases successfully catalyze oxygenation reactions including the aromatic bond cleavage under mild reaction conditions. Catechol dioxygenases possess a nonheme iron complex in the active center, which plays important roles in the oxygenation catalysis. They are divided into two types with respect to the oxidation state of the iron center: the catechol dioxygenase with iron(III) center catalyzes 1,2-cleavage of catechol (intradiol cleavage),⁶ as shown in Scheme 1A, and the other with iron(II) center catalyzes 2,3-cleavage (extra-di-ol cleavage),⁷ as shown in Scheme 1B. Though the dioxygen activation by iron(II) system is well established in heme proteins, heme protein which contains the iron(III) center is not reactive to the dioxygen molecule, as well-known. In this regard, the activation mechanism of dioxygen molecule by the iron(III) catechol dioxygenase is of considerable interest.

In the iron(III) catechol dioxygenase, the active site contains mononuclear iron(III) center, two histidine residues (His460 and

SCHEME 1: Catalytic Reaction of Catechol Dioxygenase



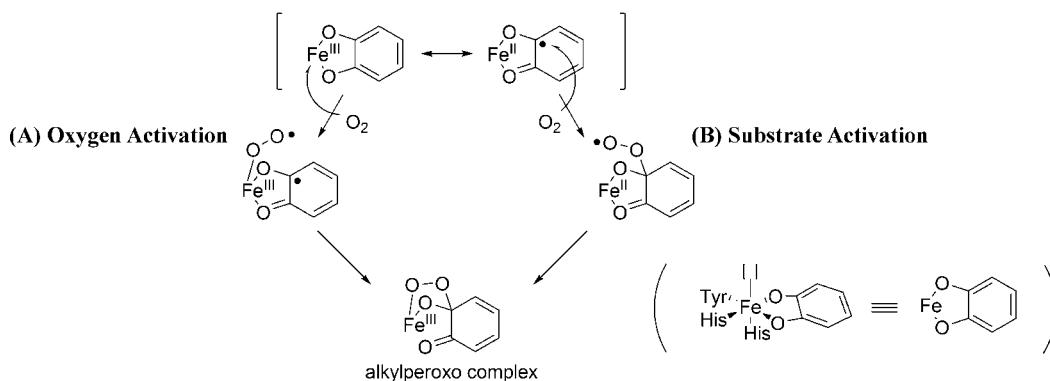
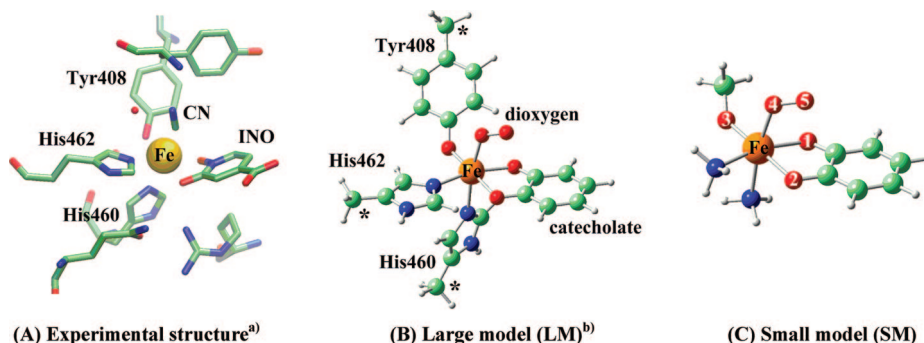
His462), two tyrosine residues (Tyr408 and Tyr447), and water molecule.^{8,9} The substrate catechol coordinates to the iron center with concomitant dissociation of Tyr447 and water molecule, to form distorted square pyramidal structure.¹⁰ Then, the dioxygen molecule approaches the active center and the oxygenation reaction of catechol occurs to produce *cis,cis*-muconic acid. Interestingly, it is known that the iron center keeps high-spin character during the catalytic cycle.^{11,12}

The oxygenation reaction and its catalytic mechanism of intradiol cleavage have been well established for decades.^{13–18} In the O₂ binding step, however, two different reaction courses were proposed: one is called “oxygen activation”^{15,19–21} and the other is called “substrate activation”.^{16–18} In the oxygen activation mechanism, dioxygen molecule attacks the iron(III) center to form an iron–dioxygen complex, in which the charge transfer occurs from the catecholate moiety to the dioxygen moiety to afford iron(III)–superoxo complex, as shown in Scheme 2A. In the substrate activation mechanism, the charge transfer occurs from the catecholate moiety to the iron(III) center to produce

* Corresponding author. E-mail: sakaki@moleng.kyoto-u.ac.jp.

[†] Graduate School of Engineering, Kyoto University.

[‡] Fukui Institute for Fundamental Chemistry, Kyoto University.

SCHEME 2: Dioxygen Activation Mechanism Previously Proposed^{15–21}SCHEME 3: (A) Experimental Structure¹⁰ of the Active Site in Iron(III) Catechol Dioxygenase, (B) Large Model (LM), and (C) Small Model (SM)^a

^a Key: (a) INO represents 2-hydroxyisonicotinic acid *N*-oxide. CN and INO are the inactive substrates mimicking dioxxygen molecule and protocatechuic acid, respectively. (b) In LM, the asterisk represents the C_{β} atoms whose positions were fixed to those of the experimental structure.

the iron(II)–semiquinonate radical,¹⁸ which reacts with the dioxxygen molecule to form a C–O bond between dioxxygen molecule and catecholate carbon atom, as shown in Scheme 2B. From kinetic studies, the O_2 binding process rapidly occurs with the rate constant of $5 \times 10^5 \text{ M}^{-1} \text{ s}^{-1}$ in the native protocatechuic-3,4-dioxygenase (3,4-PCD) from *Pseudomonas putida*.²² From recent spectroscopic studies, the iron–catecholate complexes are in equilibrium between the low-spin and high-spin states at low temperature. Interestingly, it was experimentally suggested that the low-spin state prefers the iron(II)–semiquinonate form but the high-spin state prefers the iron(III)–catecholate form.¹⁹ Also, the O_2 binding process is reversible,²³ which is considered to be consistent with the formation of iron(III)–superoxo complex in the oxygen activation mechanism. Funabiki and co-workers^{24,25} theoretically investigated the activation process with the UHF method and suggested that the oxygen activation mechanism is likely. Siegbahn and co-workers²⁶ theoretically investigated the whole catalytic cycle of intra-diol cleavage with the DFT method, where the dioxxygen binding with iron(III) center was proposed in the intermediate. They also reported that the dioxxygen attack to the catecholate carbon needed much larger activation barrier. On the other hand, the MCD spectroscopic and another DFT theoretical studies²⁷ suggested that the iron center has the intermediate spin state ($S = 3/2$) through the antiferromagnetic coupling between the dioxxygen molecule and the iron center, which induced spin-forbidden attack of O_2 on the catechol carbon atom. These suggestions support the substrate activation mechanism. Thus, the final conclusion has not been presented yet about the activation mechanism.

The detailed investigation about such approaching process provides us direct answer about the activation mechanism. In

previous theoretical studies, however, the approaching process of dioxxygen molecule to the iron(III)–catecholate complex has not been investigated well. Moreover, multireference post-Hartree–Fock method, such as CASSCF/CASPT2 method, has not been employed to investigate the activation process of dioxxygen molecule, though multiconfigurational character must be taken into consideration of the interaction between iron and dioxxygen molecule.

In this paper, we theoretically investigated the dioxxygen activation process in the iron(III) catechol dioxygenase. We employed here complete active space self-consistent-field (CASSCF) method^{28,29} and its second-order perturbation theory^{30,31} (CASPT2) to directly evaluate the multiconfigurational character of the Fe– O_2 interaction. Our main purposes are to present clear conclusion about the activation mechanism of dioxxygen molecule, and to clarify how dioxxygen molecule is activated by the iron(III) center and what roles the iron(III) center and the catecholate substrate play in the activation process.

Models and Computational Details

We employed here two computational models based on the experimental structure of protocatechuic-3,4-dioxygenase from *Pseudomonas putida* coordinated with cyanide (PDB-ID = 3PCL).¹⁰ As shown in Scheme 3A, the active site consists of Fe, 2-hydroxyisonicotinic acid *N*-oxide (INO), CN, His460, His462, and Tyr408.^{32,33} In this structure, the INO and CN are included as the inhibitors instead of the 3,4-protocatechuic (3,4-dihydroxybenzoate) and dioxxygen molecule, respectively. Considering the large computational costs of the CASSCF and CASPT2 calculations, we employed two models, “large model (LM)” and “small model (SM)”, where INO and CN were

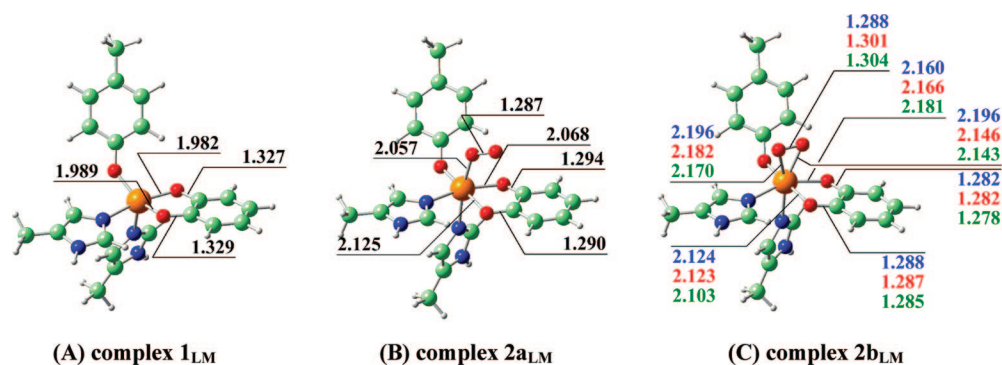


Figure 1. Optimized structures and important bond lengths (Å) of (A) iron(III)–catecholate complex $[\text{Fe}(\text{CAT})(\text{MeIm})_2(\text{MePhO})]$ 1_{LM} in sextet spin state, (B) end-on type iron(III)–superoxo complex $[\text{Fe}(\text{CAT})(\text{MeIm})_2(\text{MePhO})(\text{O}_2)]$ $2a_{LM}$ in sextet spin state, and (C) side-on type iron(III)–superoxo complex $2b_{LM}$ in octet (blue), sextet (red), and quartet (green) spin states, where CAT, MeIm, and MePhO represent catecholate, 4-methylimidazole, and 4-methyl phenoxide, respectively, which are the models of protococatechuate, histidine, and tyrosine, respectively.

substituted for catecholate and dioxygen molecule, respectively, as shown in Scheme 3B. In **LM**, amino chains of His460, His462, and Tyr408 were removed, where the positions of the C_β atoms of His460, His462, and Tyr408 were fixed to those of the experimental structure and the C_β atoms were capped by hydrogen atoms. The direction of the C_β –H bond was taken to be the same as the C_α – C_β bond of the experimental structure and its C_β –H distance was optimized. In **SM**, His462 and His460 were substituted for ammonia (NH_3) and Tyr408 was substituted for methoxide (OCH_3), as shown in Scheme 3C. The geometry of **SM** was taken to be the same as that of the corresponding moiety of **LM**. We employed **LM** in geometry optimization with the DFT method and **SM** in energy evaluation with the CASSCF and CASPT2 methods.

The geometry of **LM** was optimized by unrestricted density functional theory (UDFT) with B3LYP^{34–36} functional in each spin state. We used (311111/22111/411/1) basis set for Fe with effective core potential (ECP) for 10 core electrons³⁷ and 6-31G* basis sets for C, N, O, and H, where diffuse functions of [1s1p] were added to O. This basis set system is called BAS-I hereafter. Better basis sets were used in energy evaluation; 6-311G* basis sets were used for C, N, O, and H, where diffuse functions of [1s1p] were added to O, while the same basis set as that of BAS-I was used for Fe. This basis set system is called BAS-II.

In CASSCF calculation, we employed the active space with nine electrons in eight orbitals such as five d orbitals of Fe (d_{Fe}), π orbital of catecholate (π_{CAT}), and two π^* orbitals of O_2 (π_p^* and π_v^*), where the subscripts p and v represent the π^* orbital in the Fe–O–O plane and that vertical to the Fe–O–O plane, respectively. This CASSCF calculation is called CASSCF(9,8) hereafter. In energy evaluation, state-specific (SS) CASSCF/CASPT2 and state-averaged (SA) CASSCF/CASPT2 methods were employed, where the CASSCF wave function was employed to evaluate Mulliken charge and Mulliken spin population. We preliminarily carried out several SA-CASSCF calculations to check whether the potential energy curves are well calculated or not (see Figure S1 in Supporting Information). In those calculations, we found that three-state-averaged (3SA) CASSCF(9,8) calculation presents reliable potential energy curves for the O_2 binding process in the octet and quartet spin states. In the sextet spin state, 7SA-CASSCF(9,8) calculation presents reliable potential energy curve (see Figure S2, Supporting Information). Thus, we applied the 3SA-CASSCF(9,8)/CASPT2 method to the octet and quartet spin states, and the 7SA-CASSCF(9,8)/CASPT2 method to the sextet spin state. CASSCF(9,9), CASSCF(11,9), CASSCF(11,10), and CASSCF(11,11) calculations were carried out to check whether

the active space of 9 electrons in 8 orbitals presents correct results or not (see Supporting Information for computational details). CASSCF(9,8)/CASPT2-computed energy changes are similar to CASSCF(11,11)/CASPT2-computed ones in the octet spin state (see Figure S3, Supporting Information), indicating that the active space of 9 electrons in 8 orbitals is proper choice and CASSCF(9,8)/CASPT2-computed results are reliable.

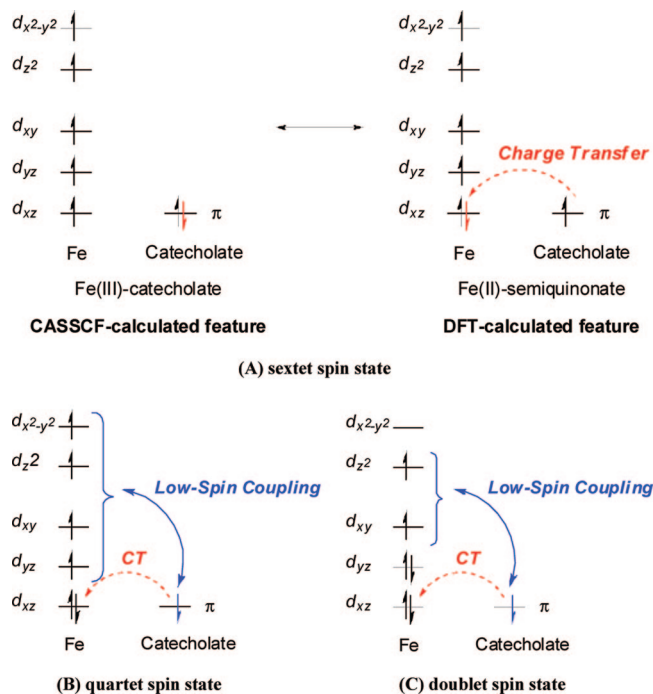
Because of the presence of intruder states, the level shift technique^{38,39} was employed in the CASPT2 calculation. The shift value was taken to be 0.20 E_h when the SS-CASSCF wave function was taken as a reference and 0.30 E_h when the SA-CASSCF wave function was taken as a reference. We examined several shift values and found that the values of 0.20 E_h and 0.30 E_h were the lowest which completely excluded the intruder states in SS-CASSCF(9,8)/CASPT2 and SA-CASSCF(9,8)/CASPT2 calculations, respectively (see Figure S4 and Figure S5, Supporting Information).

We used Gaussian03 program package⁴⁰ for DFT calculation and Molcas (version 6.4) program package⁴¹ for CASSCF and CASPT2 calculations.

Results and Discussion

The optimized structures of iron(III) catecholate complex 1_{LM} and iron(III) catecholate dioxygen complex 2_{LM} are shown in Figure 1. In 2_{LM} , we found two types of equilibrium structures; one involves η^1 -end-on coordinated dioxygen moiety ($2a_{LM}$), which is the same as the previously proposed structure,²⁶ and the other involves η^2 -side-on coordinated dioxygen moiety ($2b_{LM}$), which has not been proposed both experimentally and theoretically in the iron(III) complex. We tried to optimize iron(II) semiquinonate dioxygen intermediate which was proposed in the substrate activation mechanism, but we failed it, as will be discussed below in detail. Geometries, electronic structures, and spin states of these species will be discussed below.

Geometry, Electronic Structure, and Spin State of Iron(III) Catecholate Complex 1. The equilibrium structure of the iron(III) catecholate complex 1_{LM} in the sextet spin state is optimized with the DFT/BAS-I method, as shown in Figure 1A. This sextet spin state originates from the high spin iron(III) center. The Fe–O1 and Fe–O2 distances are 1.98 and 1.99 Å, respectively, which shows that both O atoms of catecholate strongly coordinate with the iron center. The O3 atom of Tyr408 model takes a position deviating from the *xy*-plane toward the *z*-direction. Thus, the geometry is understood to be distorted square pyramidal. The equilibrium structures of 1_{LM} in the

SCHEME 4: Electronic Structures of Complex 1 in the (A) Sextet, (B) Quartet, and (C) Doublet Spin States


quartet and doublet spin states are also optimized with the DFT/BAS-I method. The quartet and doublet spin states are calculated to be less stable than the sextet spin state by 1.5 and 22.2 kcal/mol, respectively, with the DFT/BAS-II method. Interestingly, the energy difference between the sextet and the quartet spin states is surprisingly small. It is noted that though the S^2 value (8.77) of the sextet spin state is similar to the exact value, the S^2 values (4.71 and 1.67) of the quartet and doublet spin states considerably deviate from their exact values, indicating that the spin contamination is small in the sextet spin state but large in the quartet and doublet spin states. Because the sextet spin state is the ground state in both DFT and CASPT2 calculations (see below), the spin contamination does not affect very much the equilibrium geometry of **1**.

The SS-CASSCF(7,6)/CASPT2 calculation of **1**_{SM} was carried out to investigate the energy, where the active space consists of seven electrons in five d orbitals of Fe and π orbital of catecholate. The ground state is the sextet spin state, while the quartet and doublet spin states are calculated to be much more unstable than the sextet spin state by 10.4 and 46.8 kcal/mol, respectively. In the sextet spin state of **1**_{SM}, Mulliken spin population and Mulliken charge are 4.78e and 1.06e, respectively, for the iron center, and 0.11e and $-0.85e$, respectively, for the catecholate moiety, where CASSCF wave function was employed for evaluations of Mulliken spin population and Mulliken charge, hereafter. In the catecholate moiety, Mulliken spin population and Mulliken charge are 0.01e and 0.29e, respectively, for the aromatic ring, and 0.10e and $-1.13e$, respectively, for the phenol oxygens. It is noted that the spin delocalization considerably occurs on the phenol oxygens but much less on the aromatic ring. From these results, it is clearly concluded that the iron center has high spin d^5 character, and radical character is little observed in the aromatic ring of the catecholate moiety (see Scheme 4A); in other words, **1** does not take the iron(II)–semiquinonate radical form in the sextet spin state. This is consistent with recent spectroscopic results that the iron(II)–semiquinonate radical is not formed well in

high-spin iron complex.¹⁹ Consistent with this understanding, Mulliken charge ($-0.85e$) of the catecholate moiety is much more negative than that of the quartet spin state and the d orbital population of the iron center (5.4e) is much smaller than that of the quartet spin state in which the iron(II)–semiquinonate character is involved, as will be discussed below. In the quartet spin state, Mulliken spin populations are 3.53e and $-0.58e$ and Mulliken charges are 1.12e and $-0.54e$ for the iron center and the catecholate moiety, respectively. It is noted that, though Mulliken charge of the iron center is similar to that of the sextet spin state, the d orbital population (6.1e) is much larger than that (5.4e) in the sextet spin state. These results indicate that the iron center has high spin iron(II) character and one β -spin is localized in the catechol ring in the quartet spin state (see Scheme 4B). Though this character corresponds to the iron(II)–semiquinonate species, the quartet spin state is much less stable than the sextet spin state, as described above. In the doublet spin state, Mulliken spin populations are 1.31e and $-0.32e$ and Mulliken charges are 1.07e and $-0.44e$ for the iron center and the catecholate moiety, respectively. However, the doublet spin state is much more unstable than the sextet and quartet spin states. From these results, it should be concluded that the iron(II)–semiquinonate character is little involved in the ground state (sextet spin state) of iron(III)–catecholate complex but considerably in the quartet and doublet spin states. These results are also consistent with experimental result that the low-spin state prefers the iron(II)–semiquinonate radical state.¹⁹

Iron(III) Catecholate η^1 -End-on Dioxygen Complex 2a.

The optimized structure of the iron(III) catecholate dioxygen complex **2a**_{LM} in the sextet spin state is shown in Figure 1B. In this geometry, the O4–O5 distance of the dioxygen moiety (1.29 Å) is much longer than that (1.208 Å) of free dioxygen molecule⁴² but close to that (1.3 Å) of usual superoxide.⁴³ The Fe–O4 distance is 2.06 Å and the Fe–O5 distance is 2.99 Å. These geometrical features clearly show that **2a**_{LM} is typical η^1 -end-on superoxo complex.

The geometry of **2a**_{LM} in the octet and quartet spin states could not be optimized with the DFT method, because their potential energy curves calculated with the DFT method are slightly repulsive along the Fe–O₂ distance in these spin states, as will be discussed below. Also, there is no energy minimum in these spin states. We investigated here the energy and electronic structure of **2a** in the octet and quartet spin states, using the geometry of the sextet spin state. According to the DFT/BAS-II calculation of **2a**_{LM}, the octet and quartet spin states are more stable than the sextet spin state by 2.2 and 0.2 kcal/mol, respectively. Seemingly, these results are not consistent with the O₂ binding, because these results indicated that the ground state is the octet spin state but the potential energy curve is repulsive.

Because the DFT-computed results show the very small energy difference between these spin states, we carried out SS-CASSCF(9,8)/CASPT2 calculations of **2a**_{SM} to present more detailed results about spin state.

The SS-CASSCF(9,8)/CASPT2 computations indicate that the ground state is the sextet spin state, and the octet and quartet spin states are above the sextet spin state by 3.3 and 2.8 kcal/mol, respectively, unlike the DFT-computed results. The SS-CASSCF(9,8)-computed Mulliken spin populations are 4.80e, 1.04e, and 1.05e for the iron center, catecholate, and dioxygen moieties, respectively, in the octet spin state, 4.43e, 1.03e, and $-0.56e$, respectively, in the sextet spin state, and 4.01e, $-0.55e$, and $-0.56e$, respectively, in the quartet spin state. The spin

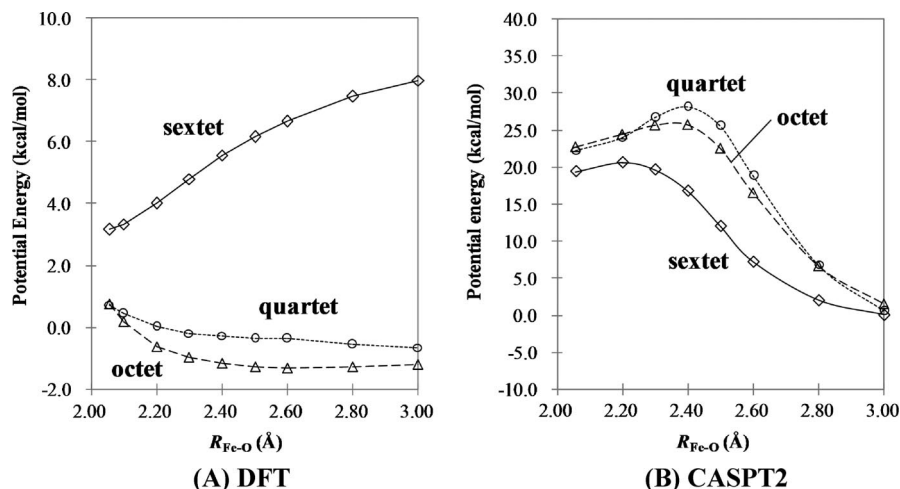
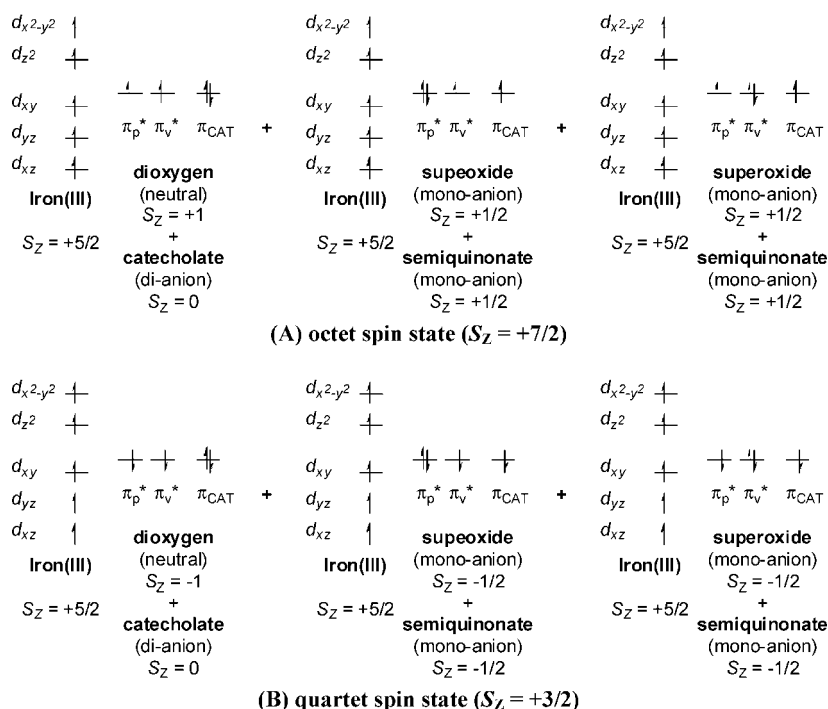


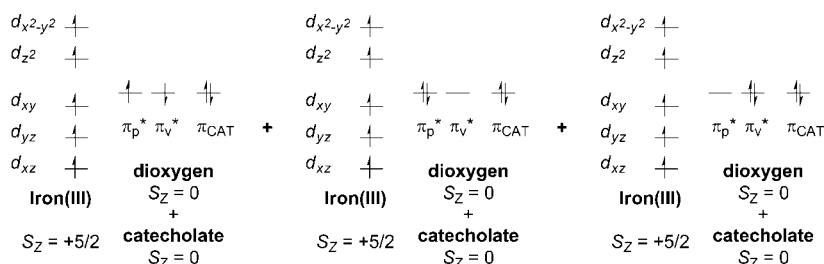
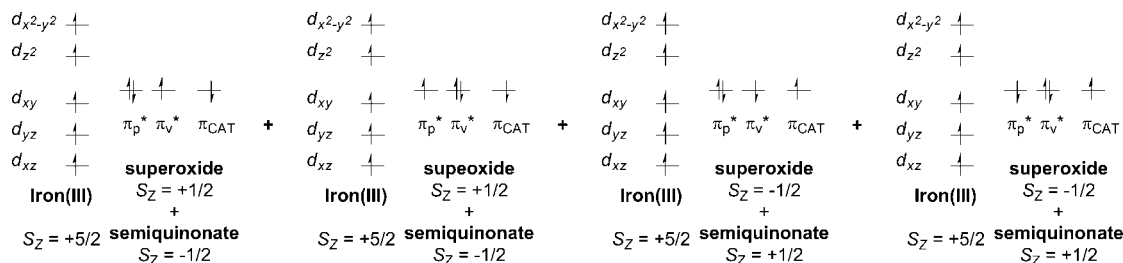
Figure 3. (A) Potential energy curves (PECs) in the O_2 binding process evaluated by the B3LYP/BAS-II method with **SM**, and (B) PECs evaluated by the 3SA-CASSCF(9,8)/CASPT2 method for the octet and quartet spin states and by the 7SA-CASSCF(9,8)/CASPT2 method for the sextet spin state with **SM**. Dashed line, solid line, and dotted line represent octet, sextet, and quartet spin states, respectively. Note that data of $R_{\text{Fe-O}} = 2.06$ Å are evaluated by CASPT2/SS-CASSCF(9,8) method with 0.20 E_h shift.

SCHEME 6: Three Electronic States Considered in the 3SA-CASSCF(9,8) Calculation of the Octet and Quartet Spin States



Considering the above results of the sextet spin state, we tried to evaluate the PEC of **SM** with the SS-CASSCF(9,8) method, where the geometry of **SM** was taken to be the same as that of the corresponding moiety of **LM**. However, this method presents unreasonable PEC for all spin states considered here; for instance, the PEC starting from **2a** cannot be connected smoothly with that starting from **1** + O_2 , suggesting the electronic state is considerably different between **1** + O_2 and **2a**; see Figure S1 in Supporting Information for this PEC. This means the SA-CASSCF method should be employed for this O_2 binding process. After preliminary SA-CASSCF calculations with several kinds of averaged states, we evaluated the PEC of **SM** with the 3SA-CASSCF(9,8) for the octet and quartet spin states and the 7SA-CASSCF(9,8) for the sextet spin state; see Figures S1 and S2 in Supporting Information and their explanation. In the octet spin state, the 3SA-CASSCF(9,8) calculation

contains one electron configuration which corresponds to iron(III) dioxygen catecholate state and two electron configurations which correspond to iron(III) superoxo semiquinonate state, as shown in Scheme 6A. We carried out the 4SA-CASSCF(9,8) calculation which contains one more electron configuration corresponding to iron(II) dioxygen semiquinonate radical state in addition to the above three electron configurations. However, this iron(II) state little influences the PEC calculated by the 3SA-CASSCF(9,8) because the iron(II) state lies at considerably higher energy than these three iron(III) states; see Figure S1C,D in Supporting Information for PECs by 3SA-CASSCF(9,8) and 4SA-CASSCF(9,8) calculations. This result indicates that the 3SA-CASSCF(9,8) calculation presents reliable PEC for the octet spin state. In the quartet spin state, the 3SA-CASSCF(9,8) calculation contains three electron configurations like the octet spin state, in which two d electrons of the iron center induce

SCHEME 7: Seven Electronic States Considered in the 7SA-CASSCF(9,8) Calculation of the Sextet Spin State**(A) Three electron configurations including singlet spin state of dioxygen moiety****(B) Four kinds of charge transfer from catecholate to dioxygen moiety**

low-spin coupling with either two π^* electrons of neutral dioxygen moiety or one π^* electron of superoxo and one π electron of semiquinonate, as shown in Scheme 6B. In the sextet spin state, on the other hand, the 3SA-CASSCF(9,8) calculation does not include all the necessary states equally, as follows: when the dioxygen moiety has the singlet spin state locally, three different electron configurations must be considered, as shown in Scheme 7. In addition to these three electron configurations, four electron configurations of charge transfer from the catecholate moiety to the dioxygen moiety must be involved in CASSCF calculation (Scheme 7). Thus, the 7SA-CASSCF(9,8) calculation was necessarily carried out to evaluate the PEC of the sextet spin state. In this 7SA-CASSCF(9,8) calculation, three electron configurations correspond to the iron(III) dioxygen catecholate states and four electron configurations correspond to the iron(III) superoxo semiquinonate radical states.

Thus, the PECs of the octet, sextet, and quartet spin states are calculated by the SA-CASSCF(9,8)/CASPT2 method. As shown in Figure 3B,⁴⁵ the energies of the octet and quartet spin states are very close to each other in all distances of $R_{\text{Fe-O}}$. The sextet spin state is more stable in energy than the octet and quartet spin states, indicating that the sextet is the ground state. This is consistent with the previous theoretical results.¹¹ Potential energy monotonously increases in all the octet, sextet, and quartet spin states, as the Fe–O distance decreases from 3.0 to 2.4 Å. Then, the energies moderately decrease in these three spin states as the Fe–O distance further decreases from 2.4 Å to **2a** ($R_{\text{Fe-O}} = 2.06$ Å).⁴⁶ These PECs are more endothermic and need larger activation barrier than expected from the fact that the enzymatic reaction occurs at room temperature. In other words, the CASPT2 method overestimates the endothermicity and the activation barrier of the O₂ binding process. On the other hand, it should be noted that the CASPT2-calculated energy of the sextet spin state is close to that of the octet spin state at the Fe–O distance of 3.0 Å, as expected. These results, as well as the smooth PEC of the sextet spin state, suggest that the CASPT2 method is useful to investigate how the electronic structure and wave function of the sextet spin state change by the approach of dioxygen molecule to the Fe complex.

Electronic Structure Changes in the O₂ Binding Process.

Mulliken charges and spin populations of the iron center, catecholate, and dioxygen moieties were evaluated by the 3SA-CASSCF(9,8) method for the octet and quartet spin states and by the 7SA-CASSCF(9,8) method for the sextet spin state, as shown in Figure 4, parts A and B, respectively. It should be noted that the Mulliken charge and spin population of the iron center are always 1.1e and 4.8e, respectively, in the octet spin state, 1.1e and 4.2e, respectively, in the sextet spin state, and 1.1e and 4.0e, respectively, in the quartet spin state, during the O₂ binding process. These results clearly indicate that the iron center keeps the high spin d⁵ character in the O₂ binding process. This feature is not consistent with the previous proposal in both substrate activation and oxygen activation mechanisms that the iron(III) center converts to the iron(II) center in the O₂ binding process; in the substrate activation mechanism proposed previously, the high-spin iron(III) center converts to high-spin iron(II) center by the charge transfer from the catecholate moiety to the iron(III) center to yield reactive semiquinonate species which possesses radical center on the catechol ring. In the oxygen activation mechanism proposed previously, the charge transfer occurs from the catecholate moiety to the iron(III) center too, so as to easily induce the charge transfer to the dioxygen moiety from the iron center.

Though the Mulliken charge and spin population of the iron center change little, the spin population of the catecholate moiety moderately increases and that of the dioxygen moiety moderately decreases in the sextet spin state as the O₂ binding proceeds (Figure 4B). At the same time, the Mulliken charge of the catecholate moiety gradually decreases and that of the dioxygen moiety gradually increases (Figure 4A). In the octet and quartet spin states, the Mulliken charges change similar to those in the sextet spin state. Though the spin population of the catecholate moiety considerably increases and that of the dioxygen moiety considerably decreases in the octet spin state, that of the catecholate moiety considerably decreases and that of the dioxygen moiety considerably increases in the quartet spin state. It is noted that though the spin population of the dioxygen moiety moderately increases and that of the catecholate moiety moderately decreases in the sextet spin state unlike those in the octet and quartet spin states (Figure 4B), Mulliken charges

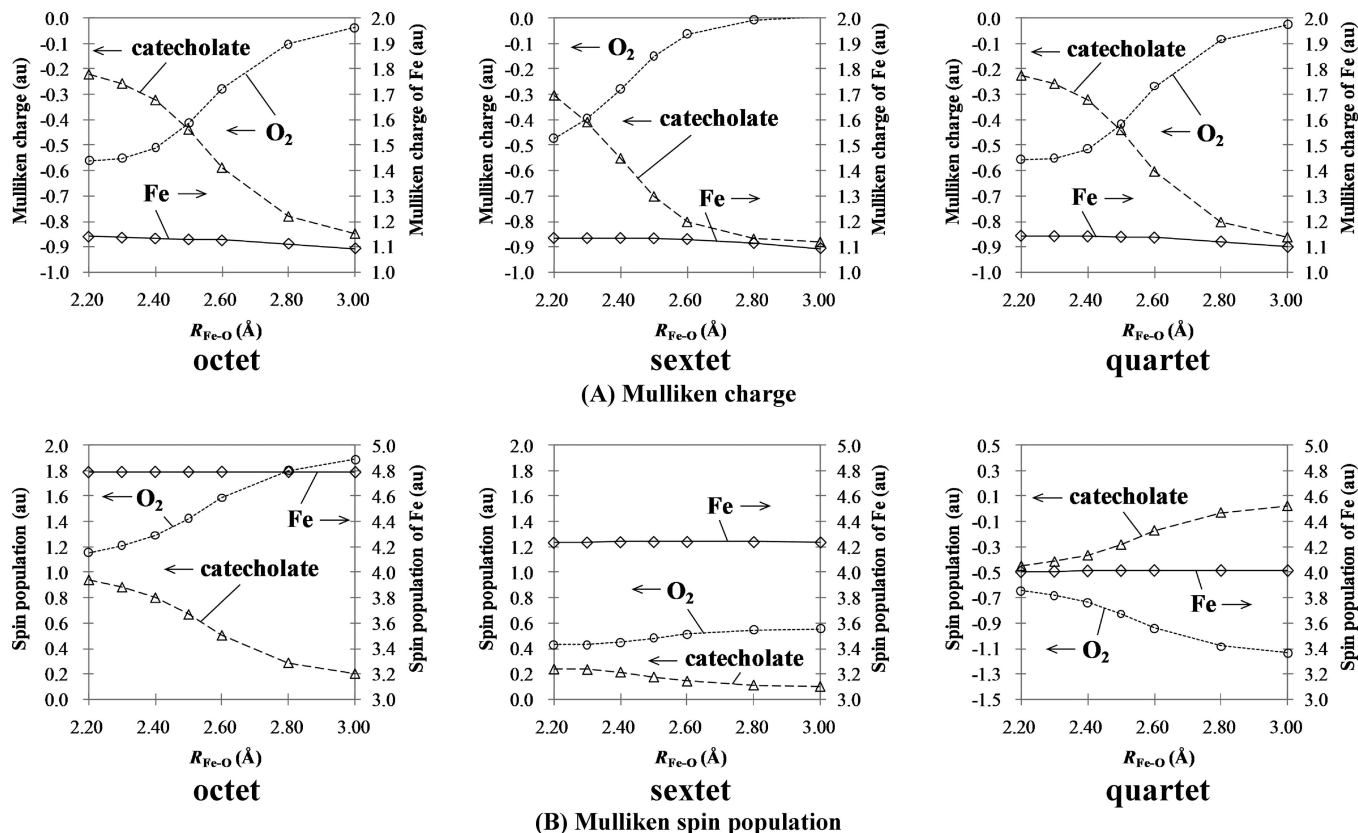


Figure 4. (A) Mulliken charges and (B) Mulliken spin populations with CASSCF method in the O₂ binding process. The 3SA-CASSCF(9,8) method was employed for the octet and quartet spin states and the 7SA-CASSCF(9,8) method was employed for the sextet spin state. Solid line, dashed line, and dotted line represent the Fe center, the catecholate, and the dioxygen moieties, respectively.

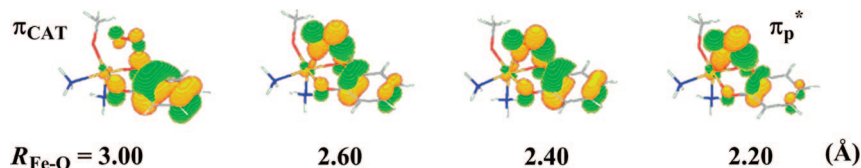


Figure 5. Natural orbital, which possesses occupation number of 2.0, evaluated by the 3SA-CASSCF(9,8) method for octet spin state.

considerably change in the sextet spin state similar to those of the octet and quartet spin states (Figure 4A). These results are consistent with the electron configurations shown in Scheme 7; in the sextet spin state, four kinds of electron configuration (Scheme 7B) participate in the charge transfer from the catecholate moiety to the dioxygen moiety, in which spin populations of the catecholate and dioxygen moieties increase in two electron configurations but decrease in the other two electron configurations. Also, the little change in Mulliken charge and spin population of the iron center indicate that the charge transfer directly occurs from the catecholate dianion taking closed-shell singlet state to the dioxygen moiety taking triplet spin state (Scheme 7), to afford finally superoxide and semiquinone monoanion which both have doublet spin state locally.

One doubly occupied natural orbital is responsible for the changes in spin and electron populations, as follows: the doubly occupied natural orbital is localized in the π orbital of the catecholate moiety at $R_{\text{Fe-O}} = 3.0$ Å, as shown in Figure 5. The π orbital of the catecholate moiety starts to interact with the π_p^* orbital of the dioxygen moiety at $R_{\text{Fe-O}} = 2.4$ – 2.6 Å, and finally, the doubly occupied orbital becomes localized in the π_p^* orbital of the dioxygen moiety at $R_{\text{Fe-O}} = 2.2$ Å. These features suggest that the π orbital of the catecholate moiety and

the π_p^* orbital of the dioxygen moiety participate in the direct charge transfer, which is consistent with the result that the Mulliken charge and spin population of the iron(III) center little change in the reaction. Interestingly, the d orbital of the iron center little participates in this orbital. This is against our expectation that the iron center plays important role in the dioxygen activation. It is of considerable importance to clarify how the iron(III) center participates in the dioxygen activation and why the iron(III) center is necessary in the O₂ binding process.

To investigate the role of the iron(III) center, we evaluate vertical electron affinities ($E_{\text{EA,v}}$) of the catecholate and dioxygen moieties with the CASPT2 method. In the evaluation of $E_{\text{EA,v}}$ of the catecholate moiety, a model complex which consisted of iron center, catecholate moiety, two ammonia ligands, and methoxide was employed. This is similar to **1**_{SM}. The SS-CASSCF(6,6)/CASPT2 and SS-CASSCF(7,6)/CASPT2 methods were applied to the septet and sextet spin states, respectively. In the evaluation of $E_{\text{EA,v}}$ of the dioxygen moiety, a model complex which consisted of iron center, catecholate moiety, dioxygen moiety, two ammonia ligands, and methoxide was employed. This is similar to **2a**_{SM}. The SS-CASSCF(8,8)/CASPT2 and SS-CASSCF(9,8)/CASPT2 methods were applied to the nonet and octet spin states, respectively. The $E_{\text{EA,v}}$ of the

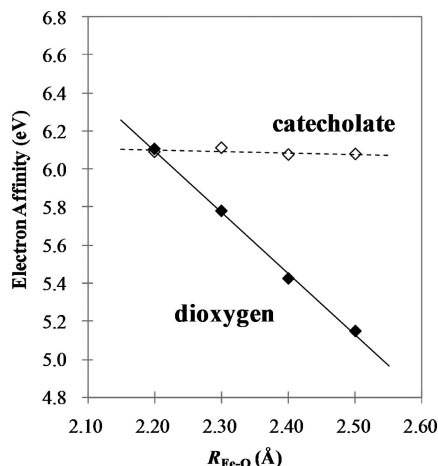
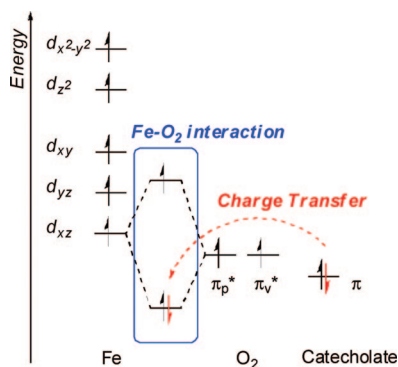


Figure 6. Vertical electron affinity of the dioxygen moiety (solid line) and the catecholate moiety (dashed line). In the catecholate moiety, the electron affinity of 1_{SM} was evaluated by the CASPT2/SS-CASSCF(6,6) and the CASPT2/SS-CASSCF(7,6) methods for the septet and sextet spin states, which correspond to the iron(III)–semiquinonate and the iron(III)–catecholate states, respectively. In the dioxygen moiety, the electron affinity of 2_{SM} were evaluated by the CASPT2/SS-CASSCF(8,8) and the CASPT2/SS-CASSCF(9,8) methods for the nonet and octet spin states, which correspond to the iron(III)–semiquinonate–neutral dioxygen and iron(III)–semiquinonate–superoxo states, respectively.

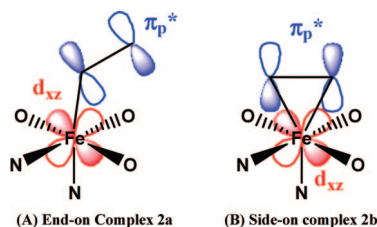
SCHEME 8: Fe–O₂ Interaction Induces the Charge Transfer from the Catecholate Moiety to the Dioxygen Moiety



catecholate moiety is always 6.1 eV, which little changes during the O₂ binding, as shown in Figure 6. On the other hand, the $E_{EA,v}$ of the dioxygen moiety considerably increases as the dioxygen molecule approaches the iron center. It is noted that the $E_{EA,v}$ of the dioxygen moiety becomes larger than that of the catecholate moiety when the Fe–O distance becomes shorter than 2.2 Å. From these results, it should be concluded that the role of iron center is “adjusting” the orbital energy of the dioxygen moiety to induce charge transfer from the catecholate moiety to the dioxygen moiety, which is schematically shown in Scheme 8.

η^2 -Side-on Coordination Superoxo Complex 2b. Unexpectedly, the side-on type iron(III)–dioxygen complex $2b_{LM}$ was optimized by the DFT method in the octet, sextet, and quartet spin states (Figure 1C). This type of iron(III) η^2 -side-on dioxygen complex has not been reported yet both theoretically and experimentally. The geometry is little different in these three spin states. The O3–O4 bond length is 1.288–1.304 Å, which is in the range of superoxide like that of $2a_{LM}$. The Fe–O3 distance is 2.170–2.196 Å and the Fe–O4 distance is 2.143–2.196 Å, indicating that the η^2 -side-on coordination mode

SCHEME 9: Bonding Interaction between the d_{xz} Orbital of the Fe Center and the π_p^* Orbital of the Dioxygen Moiety



is stable without any support such as hydrogen bond. The sextet and quartet spin states are calculated with the DFT method to be less stable than the octet spin state by 5.5 and 5.6 kcal/mol, respectively.

The SS-CASSCF(9,8)-computed Mulliken spin populations are 4.79e, 1.04e, and 1.06e for the iron center, catecholate, and dioxygen moieties, respectively, in the octet spin state, 4.55e, –0.67e, and 1.01e, respectively, in the sextet spin state, and 4.02e, –0.56e, and –0.55e, respectively, in the quartet state. From these results, it is concluded that **2b** should be characterized to be an iron(III)–superoxo complex, which is consistent with the geometrical features discussed above. The doubly occupied natural orbital involves bonding interaction between the d_{xz} orbital of Fe and the π_p^* orbital of the dioxygen moiety, as shown in Figure 2B. Though the d_{xz} orbital of Fe interacts with the π_p^* orbital in both of $2a_{SM}$ and $2b_{SM}$, the bonding interaction is different between **2a** and **2b**. In **2a**, one lobe of the d_{xz} orbital overlaps with one lobe of the π_p^* orbital in a bonding way, as shown in Scheme 9A, which is the typical bonding interaction of the η^1 -end-on type coordination of dioxygen molecule. In **2b**, on the other hand, two lobes of the d_{xz} orbital overlap well with two lobes of the π_p^* orbital in a bonding way (see Scheme 9B), which is the typical bonding interaction of the usual η^2 -side-on coordination of dioxygen molecule.

In the SS-CASSCF(9,8)/CASPT2 calculation, $2b_{SM}$ is more stable than $2a_{SM}$ by 9.1, 12.6, and 12.7 kcal/mol and more unstable than $1 + O_2$ by 13.0, 6.2, and 8.9 kcal/mol, in the octet, sextet, and quartet spin states, respectively. Also, the sextet spin state of $2b_{SM}$ is calculated to be more stable than the octet and quartet spin states by 6.8 and 2.7 kcal/mol, respectively. Thus, the ground state is the sextet spin state in both $2a_{SM}$ and $2b_{SM}$. In the DFT calculation with the same basis sets and the same geometry as those of the SS-CASSCF(9,8)/CASPT2 calculation, $2b_{SM}$ is more stable than $2a_{SM}$ by 4.1, 5.7, and 0.7 kcal/mol, in the octet, sextet, and quartet spin states, respectively. Unlike the SS-CASSCF(9,8)/CASPT2 calculation, $2b_{SM}$ is more stable than $1 + O_2$ by 2.9 and 2.6 kcal/mol in the octet and sextet spin states, respectively, but more unstable than $1 + O_2$ by 2.3 kcal/mol in the quartet spin state. Thus, the ground state is either sextet or octet spin state in $2b_{SM}$, according to the DFT calculations.

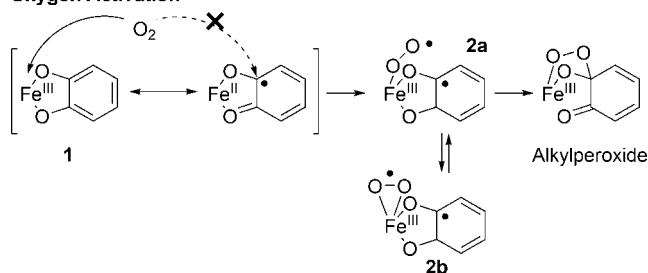
Both SS-CASSCF(9,8)/CASPT2- and DFT-computed results indicate that **2b** is a stable intermediate. It is likely that **2b** exists as a stable isomer in the early stage of the catalytic cycle of iron(III) catechol dioxygenase.

Conclusions

We carried out here the CASSCF/CASPT2 study of the dioxygen binding process in iron(III) catechol dioxygenase. Our results clearly support the oxygen activation mechanism and rule out the substrate activation mechanism, because semi-

SCHEME 10: Proposed Mechanism of the Dioxygen Activation in Iron(III) Catechol Dioxygenase

Oxygen Activation



quinonate radical character is little involved in the iron(III) catecholate complex.

We wish to present the clear feature of the dioxygen activation, as summarized in Scheme 10. First, iron(III) catecholate complex **1** is formed. In the ground state, the iron center is characterized to be high-spin d^5 species, and semiquinonate radical character is little observed, which is not enough to induce the direct reaction between the dioxygen molecule and the catechol ring. In the second step, the dioxygen molecule directly attacks the iron center to form the η^1 -end-on type Fe–O₂ complex **2a** which is understood to be iron(III) superoxo complex. O₂ binding process was investigated by the CASSCF/CASPT2 method. When dioxygen molecule is distant from the iron(III) center, the octet, sextet, and quartet spin states are nearly degenerate in the iron(III) dioxygen system (**1** + O₂). The charge transfer from the catecholate moiety to the dioxygen moiety directly occurs without formation of iron(II) character, when the Fe–O₂ distance becomes 2.4 Å or less. This is the key process of the dioxygen activation. Around the Fe–O₂ distance of 2.2 Å, the sextet spin state becomes more stable than the octet and quartet spin states. Finally, the iron(III)- η^1 -end-on superoxo species is formed, spin state of which is sextet. In this process, the Mulliken charge and spin population of the iron center little change. However, these results do not mean that the iron center does not play important role in the dioxygen activation process. The vertical electron affinity of the dioxygen moiety was calculated to be larger than that of the catecholate moiety where the Fe–O distance becomes short. This indicates that the iron center induces the charge transfer from the catecholate moiety to the dioxygen molecule by adjusting the energy level of the π_p^* orbital of O₂.

Besides **2a**, we found the iron(III)- η^2 -side-on superoxo complex **2b** as a stable intermediate, which has been neither observed nor predicted both experimentally and theoretically. These results suggest that **2b** exists in a stable isomer of earlier stage of the catalytic cycle by iron(III) catechol dioxygenase.

Acknowledgment. This study was supported in part by Grant-in-Aids on Priority Area, “Molecular Theory for Real Systems” (No. 461) and Global COE Program “International Center for Integrated Research and Advanced Education in Materials Science” (No. B-09) of the Ministry of Education, Culture, Sports, Science and Technology (MEXT) of Japan.

Supporting Information Available: Complete ref 40; model dependency; several SA-CASSCF(9,8) calculations; comparison between the CASSCF(9,8)/CASPT2 and the CASSCF(11,11)/CASPT2 calculations; LS-CASPT2 calculations using several shift values; the PECs based on the DFT-optimized geometries of the octet and sextet spin states; energy changes with protein environmental effects evaluated by the PCM method; functional

dependency in the geometry optimization; LS-CASPT2 calculations with real and imaginary level shift. This material is available free of charge via the Internet at <http://pubs.acs.org>.

References and Notes

- (1) Gibson, D. T. In *Microbial Degradation of Organic Compounds*; Marcel Dekker: New York, 1984.
- (2) Lipscomb, J. D.; Orville, A. M. In *Metal Ions in Biological Systems*; Sigel, H., Sigel, A., Eds.; Marcel Dekker: New York, 1992; Vol. 28, pp 243–298.
- (3) Funabiki, T. In *Oxygenases and Model Systems*; Funabiki, T., Ed.; Kluwer Academic Publishers: Dordrecht, The Netherlands, 1997; pp 19–104.
- (4) Costas, M.; Mehn, M. P.; Jensen, M. P.; Que, L., Jr. *Chem. Rev.* **2004**, *104*, 939–986.
- (5) Bugg, T. D. H. *Tetrahedron* **2003**, *59*, 7075–7101.
- (6) Hayaishi, O.; Katagiri, M.; Rothberg, S. *J. Am. Chem. Soc.* **1955**, *77*, 5450–5451.
- (7) Kojima, Y.; Itada, N.; Hayaishi, O. *J. Biol. Chem.* **1961**, *236*, 2223–2228.
- (8) Ohlendorf, D. H.; Lipscomb, J. D.; Webber, P. C. *Nature* **1988**, *336*, 403–405.
- (9) Ohlendorf, D. H.; Orville, A. M.; Lipscomb, J. D. *J. Mol. Biol.* **1994**, *244*, 429–440.
- (10) Orville, A. M.; Lipscomb, J. D.; Ohlendorf, D. H. *Biochemistry* **1997**, *36*, 10052–10066.
- (11) Que, L., Jr.; Lipscomb, J. D.; Zimmermann, R.; Muenck, E.; Orme-Johnson, N. R.; Orme-Johnson, W. H. *Biochim. Biophys. Acta* **1976**, *452*, 320–334.
- (12) Que, L., Jr.; Heistand, R. H., II *J. Am. Chem. Soc.* **1979**, *101*, 2219–2221.
- (13) Walsh, T. A.; Ballou, D. P.; Mayer, R.; Que, L., Jr. *J. Biol. Chem.* **1983**, *258*, 14422–14427.
- (14) Whittaker, J. W.; Lipscomb, J. D.; Kent, T. A.; Muenck, E. *J. Biol. Chem.* **1984**, *259*, 4466–4475.
- (15) Funabiki, T.; Mizoguchi, A.; Sugimoto, T.; Tada, S.; Tsuji, M.; Sakamoto, H.; Yoshida, S. *J. Am. Chem. Soc.* **1986**, *108*, 2921–2932.
- (16) Que, L., Jr.; Lipscomb, J. D.; Muenck, E.; Wood, J. M. *Biochim. Biophys. Acta* **1977**, *485*, 60–74.
- (17) Que, L., Jr.; Kolanczyk, R. C.; White, L. S. *J. Am. Chem. Soc.* **1987**, *109*, 5373–5380.
- (18) Cox, D. D.; Que, L., Jr. *J. Am. Chem. Soc.* **1988**, *110*, 8085–8092.
- (19) Funabiki, T.; Fukui, A.; Hitomi, Y.; Higuchi, M.; Yamamoto, T.; Tanaka, T.; Tani, F.; Naruta, Y. *J. Inorg. Biochem.* **2002**, *91*, 151–158.
- (20) Hitomi, Y.; Yoshida, S.; Higuchi, M.; Minami, H.; Tanaka, T.; Funabiki, T. *J. Inorg. Biochem.* **2005**, *99*, 755–763.
- (21) Higuchi, M.; Hitomi, Y.; Minami, H.; Tanaka, T.; Funabiki, T. *Inorg. Chem.* **2005**, *44*, 8810–8821.
- (22) Bull, C.; Ballou, D. P.; Otsuka, S. *J. Biol. Chem.* **1981**, *256*, 2681–2686.
- (23) Hitomi, Y.; Tase, Y.; Higuchi, M.; Tanaka, T.; Funabiki, T. *Chem. Lett.* **2004**, *33*, 316–317.
- (24) Funabiki, T.; Inoue, T.; Kojima, H.; Konishi, T.; Tanaka, T.; Yoshida, S. *J. Mol. Catal.* **1990**, *59*, 367–371.
- (25) Funabiki, T.; Yamazaki, T. M. *J. Mol. Catal. A* **1999**, *150*, 37–47.
- (26) Borowski, T.; Siegbahn, P. E. M. *J. Am. Chem. Soc.* **2006**, *128*, 12941–12953.
- (27) Pau, M. Y. M.; Davis, M. I.; Orville, A. M.; Lipscomb, J. D.; Solomon, E. I. *J. Am. Chem. Soc.* **2007**, *129*, 1944–1958.
- (28) Roos, B. O.; Taylor, P. R. *Chem. Phys.* **1980**, *48*, 157–173.
- (29) Roos, B. O. In *Ab Initio Methods in Quantum Chemistry II*; Lawley, K. P., Ed.; Wiley: New York, 1987; p 399.
- (30) Andersson, K.; Malmqvist, P.-Å.; Roos, B. O.; Sadlej, A. J.; Wolinski, K. *J. Phys. Chem.* **1990**, *94*, 5483–5488.
- (31) Andersson, K.; Malmqvist, P.-Å.; Roos, B. O. *J. Chem. Phys.* **1992**, *96*, 1218–1226.
- (32) Arginine residue (Arg457) exists close to the active site. It plays important role in the conformational change of an alkylperoxo complex which occurs after the dioxygen activation process.²⁶ However, recent theoretical study reported that the arginine residue little participates in the dioxygen activation process.²⁶ Thus, we did not consider Arg457 in our calculation models.
- (33) (a) To estimate protein environmental effects, the energies and electronic structures were also evaluated with PCM (polarized continuum model) method^{33b} at the DFT (B3LYP) level, employing dielectric constant of 4.0 and probe radius of 1.4 Å for **LM**. These results showed that the relative energies and electronic structures are little changed by the protein environment in the dioxygen activation process; see Supporting Information for details. (b) Cancès, M. T.; Mannucci, B.; Tomasi, J. *J. Chem. Phys.* **1997**, *107*, 3032–3041. Cossi, M.; Barone, V.; Mennucci, B.; Tomasi, J.

Chem. Phys. Lett. **1998**, 286, 253–260. Mennucci, B.; Tomasi, J. *J. Chem. Phys.* **1997**, 106, 5151–5158.

(34) Lee, C.; Yang, W.; Parr, R. G. *Phys. Rev. B: Condens. Matter Mater. Phys.* **1988**, 37, 785–789.

(35) Miehlisch, B.; Savin, A.; Stoll, H.; Preuss, H. *Chem. Phys. Lett.* **1989**, 157, 200–206.

(36) Becke, A. D. *J. Chem. Phys.* **1993**, 98, 5648–5652.

(37) Dolg, M.; Wedig, U.; Stoll, H.; Preuss, H. *J. Chem. Phys.* **1987**, 86, 866–872.

(38) Roos, B. O.; Andersson, K. *Chem. Phys. Lett.* **1995**, 245, 215–223.

(39) Roos, B. O.; Andersson, K.; Fülscher, M. P.; Serrano-Andrés, L.; Pierloot, K.; Merchán, M.; Molina, V. *J. Mol. Struct. Theochem.* **1996**, 388, 257–276.

(40) Frisch, M. J.; et al. *Gaussian 03, Revision C.02*; Gaussian Inc.: Wallingford, CT, 2004.

(41) Karlström, G.; Lindh, R.; Malmqvist, P.-Å.; Roos, B. O.; Ryde, U.; Veryazov, V.; Widmark, P.-O.; Cossi, M.; Schimmelpfennig, B.; Neogrady, P.; Seijo, L. *Comput. Mater. Sci.* **2003**, 28, 222–239.

(42) Herzberg, G. In *Spectra of Diatomic Molecules*, 2nd ed.; Spinks, J. W. D., Ed.; Krieger Pub. Co.: Malabar, FL, 1989.

(43) Cramer, C. J.; Tolman, W. B.; Theopold, K. H.; Rheingold, A. L. *Proc. Nat. Acad. Sci. U.S.A.* **2003**, 100, 3635–3640.

(44) The π_v orbital of the dioxygen moiety was involved in the active space instead of the π_p^* orbital in the sextet spin state. However, this is not unreasonable, as follows: because both natural orbitals (NOs) possess occupation number of 2.00, these two NOs little contribute to the correlation energy of SS-CASSCF(9,8) calculation, and therefore, the orbital order accidentally changes between these NOs.

(45) First, PECs of the octet, sextet, and quartet spin states were calculated with the DFT-optimized geometry in each spin state. However, the octet and sextet spin states calculated with the quartet geometry are more stable than those with the octet and sextet geometries. This suggests that true geometries of **2a_{SM}** in the octet and sextet spin states are more close to the DFT-optimized geometry for the quartet spin state rather than the DFT-optimized geometries for the octet and sextet states. Thus, we employed the DFT-optimized geometry for the quartet spin state to evaluate PECs of the octet and sextet spin states and to discuss their energies and electronic structures. PECs calculated with the DFT-optimized geometries for the octet and sextet spin states are presented in the Supporting Information, Figure S6.

(46) We did not present the PECs between $R_{\text{Fe-O}} = 2.20$ Å and the DFT-optimized distance of **2a** in the sextet spin state ($R_{\text{Fe-O}} = 2.06$ Å) in Figure 3, because the energy of **2a_{SM}** could not be reliably computed by the 7SA-CASSCF(9,8)/CASPT2 method, as follows: in **2a_{SM}**, higher two states in the seven electron configurations considered by 7SA-CASSCF(9,8) calculation become more unstable and cannot be involved in 7SA-CASSCF(9,8) calculation. Instead of 7SA-CASSCF(9,8) calculation, we performed SS-CASSCF(9,8)/CASPT2 calculations to examine PEC between $R_{\text{Fe-O}} = 2.20$ and 2.06 Å, because SS-CASSCF(9,8)/CASPT2 method presents reliable energy between $R_{\text{Fe-O}} = 2.06$ and 2.30 Å. The SS-CASSCF(9,8)/CASPT2-calculated PEC slightly decreases upon going from $R_{\text{Fe-O}} = 2.20$ to 2.06 Å, suggesting that **2a** is in shallow minimum and the activation barrier is near to the energy difference between $R_{\text{Fe-O}} = 3.00$ and 2.20 Å, which is about 20.5 kcal/mol.

JP806507K